Inorg. Chem. **2009**, *48*, 828−837

Inorganic Chemistry
Article

Theoretical and Spectroscopic Investigations of the Bonding and Reactivity of $(RO)_3M{\equiv}N$ Molecules, where M = Cr, Mo, and W

Shentan Chen,[†] Malcolm H. Chisholm,*[,†] Ernest R. Davidson,[‡] Jason B. English,[§] and Dennis L. Lichtenberger*[,||]

Department of Chemistry, The Ohio State University, 100 W. 18th Avenue, Columbus, Ohio 43210-1173, Department of Chemistry, University of Washington, Box 351700, Seattle, Washington 98195-17, BP Refining Technology, 150 W. Warrenville Road, Naperville, Illinois 60563, and Department of Chemistry, The University of Arizona, Tucson, Arizona 85721

Received September 18, 2008

The electronic structures of the molecules $(^tBuO)_3M{\equiv}N$ (M = Cr, Mo, W) have been investigated with gas phase photoelectron spectroscopy and density functional calculations. It is found that the alkoxide orbitals mix strongly with the M≡N triple bond orbitals and contribute substantially to the valence electronic structure. The first ionization of $(^tBuO)_3Cr{\equiv}N$ is from an orbital of $a_2(C_{3v})$ symmetry that is oxygen based and contains no metal or nitrogen character by symmetry. In contrast, the first ionizations of the molybdenum and tungsten analogues are from orbitals of a_1 and e symmetry that derive from the highest occupied M≡N σ and π orbitals mixed with the appropriate symmetry combinations of the oxygen p orbitals. In this a_1 orbital, the oxygen p orbitals mix with the highest occupied M≡N orbital of σ symmetry. This mixing reduces the metal character, consequently reducing the metal−nitrogen overlap interaction in this orbital. From computational modeling, the polarity of the M≡N bond increases down the group such that W≡N has the highest charge separation. In addition to investigation of the effects of the metals, the electronic influences of substitution at the alkoxide ligands have been examined for the molecules $(RO)_3Mo{\equiv}N$ (R = $C(CH_3)_2H$, $C(CH_3)_3$, and $C(CH_3)_2CF_3$). The introduction of CF_3 groups stabilizes the molecular orbital energies and increases the measured ionization energies, but does not alter the overall electronic structure. The bonding characteristics of the $(^tBuO)_3M{\equiv}N$ series are compared with those of organic nitriles.

Introduction

Spurred by the discovery of metal−alkylidyne complexes that are active as catalysts for alkyne metathesis reactions, the interest in compounds containing metal−heteroatom multiple bonds has increased rapidly in the last 20 years.[1−6] Transition metal−organic and transition metal−heteroatom multiple bonds are functional groups with diverse reactivities, ranging from stabilizing metals in high oxidation states to serving as the center of reactivity in a molecule.[5] Some common reactions involving the metal−heteroatom bond include atom or group transfer reactions and metathesis reactions.[7−11] The reactivity of metal−heteroatom molecules is greatly influenced by the metal, the electron configuration of the metal, and the particular set of attendant ligands. In

* To whom correspondence should be addressed. E-mail: chisholm@chemistry.ohio-state.edu (M.H.C.), dlichten@email.arizona.edu (D.L.L.).
† The Ohio State University.
‡ University of Washington.
§ BP Refining Technology.
|| The University of Arizona.

(1) Caulton, K. G.; Chisholm, M. H.; Doherty, S.; Folting, K. *Organometallics* **1995**, *14*, 2585.
(2) Blau, R. J.; Chisholm, M. H.; Eichorn, B. W.; Huffman, J. C.; Kramer, K. S.; Lobkowsky, E. B.; Streib, W. E. *Organometallics* **1995**, *14*, 1855.
(3) Baxter, D. V.; Chisholm, M. H.; Distasi, V. F.; Haubrick, S. T. *Chem. Mater.* **1995**, *7*, 84.
(4) Chisholm, M. H.; Foltingstreib, K.; Tiedtke, D. B.; Lemoigno, F.; Eisenstein, O. *Angew. Chem., Int. Ed.* **1995**, *34*, 110.
(5) Mayer, J. M.; Nugent, W. A. *Metal-Ligand Multiple Bonds: the Chemistry of Transition Metal Complexes Containing Oxo, Nitrido, Imido, Alkylidene, or Alkylidyne Ligands*; John Wiley & Sons: New York, 1988.
(6) Wang, X.; Andrews, L.; Lindh, R.; Veryazov, V.; Roos, B. O. *J. Phys. Chem. A* **2008**, *112*, 8030.
(7) (a) Burroughs, B. A.; Bursten, B. E.; Chen, S.; Chisholm, M. H.; Kidwell, A. R. *Inorg. Chem.* **2008**, *47*, 5377. (b) Chisholm, M. H.; Delbridge, E. E.; Kidwell, A. R.; Quinlan, K. R. *Chem. Commun.* **2003**, 126.

10.1021/ic801786u CCC: $40.75
Published on Web 12/19/2008

traversing the transition elements from group 4 to group 10, one finds that the electronegativity increases and one encounters, with increasing d^n electron count, what has been described as an "OXO wall" after which multiple bonding is not favored. Also, early transition metal terminal oxo groups are considered nucleophilic while for the later elements in their high oxidation states they have been considered electrophilic. To a lesser extent, the same considerations have been applied to the terminal metal−nitride ligand. Nucleophilic nitrides of the early transition elements are often subject to hydrolysis yielding ammonia while the nitrides of high valent group VII−VIII elements have been shown to react with tertiary phosphine, carbanions, dienes, and thiolates.[12−15] In this work, we examine the electronic structure of a series of tris-alkoxide group 6 transition metal−nitrido molecules. The effect of the metal on the electronic structure is observed in (^{t}BuO)$_3$M≡N where M is Cr, Mo, or W, and the effect of substitutions on the alkoxides is observed in the series of molecules (RO)$_3$Mo≡N where R is ^{t}Bu, ^{i}Pr, or CF$_3$Me$_2$C.[16−18] The combination of gas phase UV photoelectron spectroscopy and calculations employing density functional theory provides insight into the nature of the frontier molecular orbitals in the series of compounds and the electron distribution within the M≡N bond. A comparison is also made with simple organic nitriles.

Results and Discussion

General Bonding Considerations. Unlike dinitrogen and organic nitriles, the multiple bonds to nitrogen in metal−nitrido molecules involve metal d orbitals, which are also involved in interactions with the attendant ligands. As a first step in considering the metal interactions with the alkoxides, the oxygen donors simply serve to determine the relative ordering of the d orbitals. The effect of the σ donor orbitals of the alkoxides on the d orbitals is shown on the left side of Figure 2 for a typical (RO)$_3$M fragment. The ligand σ donor orbitals form a_1 and e symmetry combinations, as illustrated in **1** below for the oxygen p orbitals directed at the metal. The ligand e symmetry orbitals in **1** mix with the two sets of metal e symmetry orbitals, the $d_{x^2-y^2}$, d_{xy} and d_{xz}, d_{yz}. The resulting upper e orbitals on the left of Figure 2 are the antibonding counterparts of M−L σ bonds. At the trigonal N≡M−O angle of ∼101−108° for these alkoxides,[16,17,24] these orbitals are primarily $d_{x^2-y^2}$, d_{xy} in character with smaller amounts of d_{xz}, d_{yz}. The lower e orbitals on the left of Figure 1 are mostly nonbonding and primarily d_{xz}, d_{yz} in character. The ligand a_1 combination in **1** mixes with the metal d_{z^2} orbital to destabilize the predominantly d_{z^2} orbital. The resultant order of the predominantly metal fragment orbitals is then d_{xz}, $d_{yz} \leq d_{z^2} < d_{x^2-y^2}$, d_{xy}, which is the same as the crystal field splitting of d orbitals for the trigonal angles of these alkoxides.

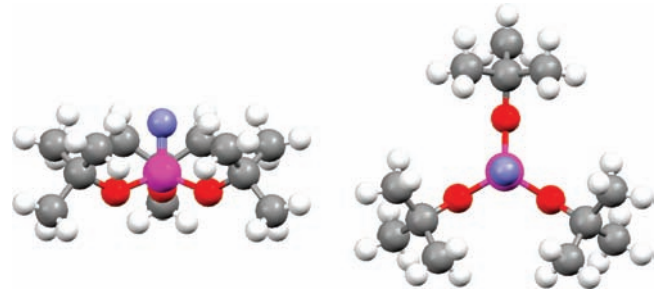

Figure 1. Side and top (down the N−Cr bond) views of the crystal structure[16] of (^{t}BuO)$_3$Cr≡N showing the C_{3v} symmetry.

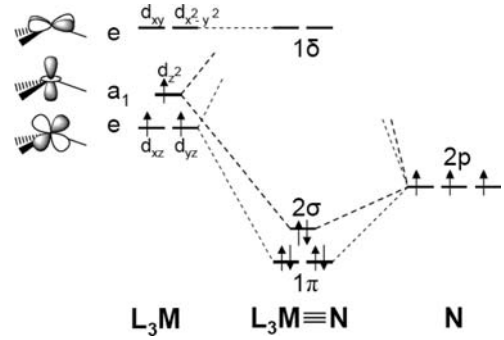

Figure 2. Orbital interaction diagram of a d^3-L$_3$M fragment, where L is a simple σ donor ligand (left), with the N(p) orbitals (right). The L−M−L angle is ∼110−116° for these molecules.

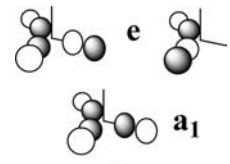

1

A qualitative representation of the interaction of these L$_3$M fragment orbitals with the nitrogen p orbitals is shown in the middle of Figure 2. The HOMO is designated with the label 2σ, and the SHOMO is labeled 1π. The 1π orbital is formed primarily from interaction of the N pπ orbitals with the predominantly metal d_{xz}, d_{yz} orbitals, and further mixing with the predominantly metal $d_{x^2-y^2}$, d_{xy} orbitals is ignored in the diagram. This order of 2σ above 1π is partly a

(8) (a) Geyer, A. M.; Wiedner, E. S.; Gary, J. B.; Gdula, R. L.; Kuhlmann, N. C.; Johnson, M. J. A.; Dunietz, B. D.; Kampf, J. W. *J. Am. Chem. Soc.* **2008**, *130*, 8984. (b) Gdula, R. L.; Johnson, M. J. A. *J. Am. Chem. Soc.* **2006**, *128*, 9614. (c) Gdula, R. L.; Johnson, M. J. A.; Ockwig, N. W. *Inorg. Chem.* **2005**, *44*, 9140.
(9) Cherry, J.-P.F.; Johnson, A. R.; Baraldo, L. M.; Tsai, Y.-C.; Cummins, C. C.; Kryatov, S. V.; Rybak-Akimova, E. V.; Capps, K. B.; Hoff, C. D.; Harr, C. M.; Nolan, S. P. *J. Am. Chem. Soc.* **2001**, *123*, 7271.
(10) Bendix, J. *J. Am. Chem. Soc.* **2003**, *125*, 13348.
(11) Woo, K. L.; Goll, G. J.; Czapla, D. J.; Hays, A. J. *J. Am. Chem. Soc.* **1991**, *113*, 8478.
(12) (a) Wong, T.-W.; Lau, T.-C.; Wong, W.-T. *Inorg. Chem.* **1999**, *38*, 6181. (b) Chiu, S.-M.; Wong, T.-W.; Man, W.-T.; Wong, W.-T.; Peng, S.-M.; Lau, T.-C. *J. Am. Chem. Soc.* **2001**, *123*, 12720. (c) Chan, P.-M.; Yu, W.-Y.; Che, C.-M.; Cheung, K.-K. *J. Chem. Soc., Dalton Trans.* **1998**, 3183.
(13) Crevier, T. J.; Bennett, B. K.; Soper, J. D.; Bowman, J. A.; Dehestani, A.; Hrovat, D. A.; Lovell, S.; Kaminsky, W.; Mayer, J. M. *J. Am. Chem. Soc.* **2001**, *123*, 1059.
(14) Maestri, A. G.; Cherry, K. S.; Toboni, J. J.; Brown, S. N. *J. Am. Chem. Soc.* **2001**, *123*, 7459.
(15) Huynh, M. V.; White, P. S.; Meyer, T. J. *J. Am. Chem. Soc.* **2001**, *123*, 9170.
(16) Chui, H. T.; Chen, Y. P.; Chuang, S. H.; Jen, J. S.; Lee, G. H.; Peng, S. M. *Chem. Commun.* **1996**, 139.
(17) Chan, D. M. T.; Chisholm, M. H.; Folting, K.; Huffman, J. C.; Marchant, N. S. *Inorg. Chem.* **1986**, *25*, 4170.
(18) Schrock, R. R.; Listemann, M. L.; Sturgeoff, L. G. *J. Am. Chem. Soc.* **1982**, *104*, 4291.

(19) All % characters are from ADF 2007.01 geometry optimizations.

consequence of the N(2s) contributions to this M≡N σ orbital, similar to the description of the bonding in HCN and CH_3CN. From ADF calculations, the N(2s) contributions to the highest occupied orbital of σ symmetry of these molecules is on the order of 30%.[19] An additional reason for the destabilization of the 2σ relative to the 1π is the contribution from the ligand a_1 orbital shown on the left of Figure 2. For the purposes of the present work, the splitting of the 2σ and 1π orbitals from these interactions is small, particularly in comparison to the effects of the oxygen π donor orbitals discussed next. As one additional contrast to nitrogen triple bonds in organic nitriles, the lowest unoccupied molecular orbitals are the predominantly metal $d_{x^2-y^2}$ and d_{xy} orbitals labeled 1δ rather than the C−N π^* orbitals of organic nitriles.

Alkoxide π-Donor Effects. Discussion of the effects of the oxygen π donor orbitals on the electronic structure could be continued in terms of the interaction of the $(RO)_3M$ fragment with a nitrogen atom. However, as will be seen, the effects of the oxygen π donor orbitals are much more significant than a simple perturbation of the character and relative energy of the predominantly metal d orbitals. An alternative approach is to view the system in terms of $(RO)_3$ and M≡N fragments. This approach separates the alkoxide ligand framework (the constant in the system) from the variable M≡N framework. Hence, it allows ready analysis of the effects of M substitution on the electronic structure of the system. Conversely, for the $(RO)_3$ Mo≡N molecules where the alkoxide is varied, the constant Mo≡N framework is separated from the alkoxide framework so that the effects of alkoxide substitution on the electronic structure can be effectively probed.

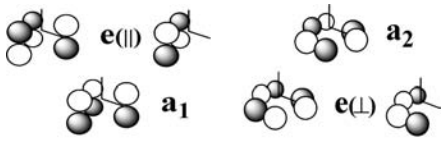

2 3

For simplicity, the oxygen p orbitals that are π with respect to the metal are separated into two groups: those parallel to the M≡N framework and those perpendicular to the M≡N framework. The parallel combinations a_1 and e(||) are shown in **2**. The a_1 combination has reasonable overlap with the M≡N σ orbital, and the e(||) combination has reasonable overlap with the M≡N π orbitals. The perpendicular ligand combinations a_2 and e($\perp$) shown in **3** will interact much less significantly with the M≡N orbitals. In fact, by symmetry the a_2 combination does not interact with the M≡N orbitals at all. The relative ordering of the six oxygen pπ combinations (a_1 < e($\perp$) < e(||) < a_2) follows from the nodal and overlap properties of the orbitals. The e($\perp$) and e(||) combinations, being of the same symmetry, may further mix and split with each other. Most important, it should be noted that the a_2 orbital is completely antibonding and is the most destabilized of the combinations.

A qualitative molecular orbital diagram illustrating the interactions of the $(RO)_3$ π-type combinations with the M≡N

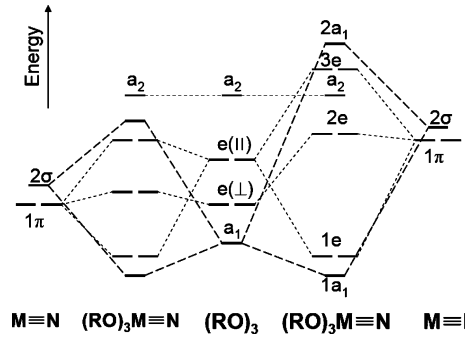

Figure 3. Molecular orbital energy diagram showing the interactions between the six highest occupied π-type combinations of the $(RO)_3$ fragment (middle) and M≡N 2σ and 1π orbitals with two different energies relative to the $(RO)_3$ orbitals, left and right, of the M≡N orbitals.

orbitals is presented in Figure 3. The diagram presents two possibilities with regards to the relative energies of the M≡N fragment orbitals and the ligand orbitals. On the right of the diagram the relative energies and interactions of the M≡N orbitals with the alkoxide orbitals are such that the $2a_1$ and 3e orbitals become the highest occupied. On the left of the diagram, the M≡N orbitals are more stable, and the alkoxide a_2 orbital becomes the highest occupied. Depending on the particular transition metal, the actual electronic structure of the $(RO)_3M$≡N molecules may correspond to either description. The relative ordering and character of the orbitals is the subject of the present photoelectron and computational studies. Regardless of the relative energies, the ligand a_1 and e(||) orbitals form bonding and antibonding combinations with the M≡N σ and π orbitals, respectively. Hence, the definitions of localized M≡N σ and π orbitals are no longer valid because of significant orbital mixing with the strong π donor ligand orbitals. We will label the occupied valence molecular orbitals of the $(RO)_3M$≡N molecules according to the designations given in Figure 3. Note that the top cluster, $2a_1$, 3e, a_2, and 2e, are all either antibonding between the M≡N orbitals and the oxygen donor orbitals or antibonding between the oxygen donor orbitals themselves (the a_2). In contrast, the lower set of orbitals, the 1e and $2a_1$, are bonding both within the M≡N orbitals and between M≡N orbitals and the oxygen donor orbitals. An energy gap between the antibonding and bonding sets is expected.

The orbital interaction diagram, Figure 3, assumes that the relative energies of the ligand symmetry combinations remain constant as the metal is changed. However, as the metal−oxygen distances decrease (M = W ≈ Mo > Cr), the distances between the oxygen atoms also decrease and the intramolecular interactions between the oxygen atoms increase. The spread of the ligand symmetry orbitals will be greatest for the $(RO)_3Cr$≡N molecule because the bonding or antibonding nature of each particular symmetry orbital becomes more important as the overlap between the oxygen p orbitals increases. With this in mind, the ligand a_2 combination will be least stable for the distances between the oxygen atoms in the Cr molecule and more stable for the distances in the Mo and W molecules.

Electronegativity Consideration. Some trends in the orbital stabilities and characters may be anticipated from the relative electronegativity of the atoms. For instance, in the cases of HC≡N, and CH_3C≡N, the N atom is more

electronegative than the C atom, so the highest occupied σ and π orbitals are polarized toward N, but otherwise correspond directly to the $2\sigma_g$ and $1\pi_u$ orbitals of N_2. Simply put, both hydrogen cyanide and acetonitrile are better σ donors than N_2. The lower electronegativities of the metal atoms would by themselves suggest similar polarizations in the transition metal−nitrido molecules, but the effects of the attendant ligand on the metal must also be taken into account. The electronegativities of the transition metals decrease as a group is descended: Cr(VI) = 3.37, Mo(VI) = 2.20, and W(VI) = 1.67.[20] Therefore, the description of the Cr molecule would be expected to lie to the left of the descriptions of the Mo and W molecules in the interactions depicted in Figure 2. On the basis of these considerations, ionizations containing substantial M≡N σ and π character should decrease in energy as M = Cr > Mo > W. The M≡N polarity as well as the N atom basicity should increase as the group is descended (M = Cr < Mo < W).

The orbital framework developed thus far is sufficient for discussion of the photoelectron spectra. The description to this stage has not included the full set of atomic functions or the effects of mixing the oxygen p orbitals with the alkyl σ framework. These interactions, which will be discussed in the computational section following analysis of the photoelectron spectra, have lesser influence on the relative energies, bonding, and polarity of the orbitals that make up the metal−nitride triple bond in these *tris*-alkoxide complexes.

Photoelectron Spectroscopic Studies. Just as in the studies of triple bonds to nitrogen in simpler molecules, photoelectron spectroscopy helps to quantify the nature of the orbital interactions and the trends in energies in metal−nitrides discussed in the previous section. The He I photoelectron spectra of the (^{t}BuO)$_3$M≡N (M = Cr, Mo, or W) molecules in the 8.5−15.0 eV ionization energy range are presented in Figure 4. For comparison, the spectrum of ^{t}BuOH is included. The ^{t}BuOH spectrum provides a benchmark for understanding the contribution of the alkoxide ligands to the (^{t}BuO)$_3$M≡N spectra. The alcohol spectrum consists of three distinct regions in the 10−15 eV range. Band A at 10.22 eV derives from the oxygen p orbital (lone pair) that is perpendicular to the C−O−H plane, and band B derives from the oxygen p orbital (long pair) that is in the C−O−H plane, bisecting the C−O−H angle. Both are strongly mixed with the C−C and C−H σ bonds of the t-butyl group, and the in-plane orbital is additionally mixed with the O−H σ bond. The different mixings, particularly with the O−H bond, account for the different energies of the ionizations. The mixing in band B is more bonding in nature than the mixing in band A, as evidenced by the width of the ionization band. Band C can be assigned to the O−C(σ), the C−C(σ), as well as the C−H(σ) ionizations.

The ionizations of the alcohol are related to those of the alkoxides by removing the hydroxyl proton from the alcohol and placing the resulting alkoxide on the metal. In a stepwise process, removal of the proton produces an alkoxide with

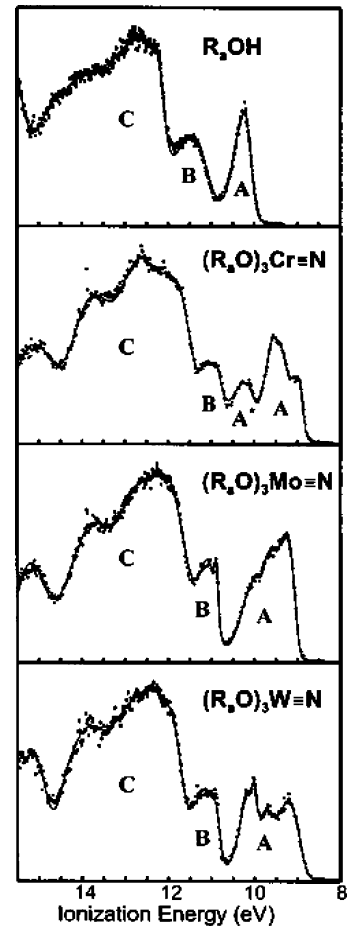

Figure 4. He I photoelectron spectra of ROH and (RO)$_3$M≡N (M = Cr, Mo, or W; R = ^{t}Bu).

3-fold symmetry (C_{3v}), and the oxygen-based ionization that was in band B, which was stabilized by overlap with the H(1s) function, becomes degenerate with band A in an e symmetry pair that is predominantly the oxygen p_x and p_y orbitals (assuming the *z*-axis is along the 3-fold symmetry axis). The loss of stabilization provided by the proton in comparison to the metal destabilizes all of the alkoxide ionizations relative to the alcohol. Judging by the shift of band C from the alcohol to the alkoxide spectra, the predominantly oxygen p_x and p_y ionizations will be about 10 eV before overlap interactions with the M≡N and neighboring ligand orbitals in the molecule. These interactions produce the spread of ionizations from 8.5 to 11.5 eV in the spectra of the *tris*-alkoxide metal−nitride molecules. The spread of 3 eV indicates substantial interaction.

Metal Substitution. One of the most helpful means of assigning ionizations is to look at a series of molecules with the same ligand set but different transition metals, because ionizations from metal-based orbitals will shift as the metal is changed. Looking at the spectra of the transition metal nitrides, we can once again separate the spectra into three separate regions: A + A* (8.5−10.5 eV), B (10.5−11.5 eV), and C (11.5−15.0 eV). Region C is essentially the same as M is changed, implying the region is dominated by ionizations from ligand-based orbitals. The region contains the C−C(σ), the C−H(σ), as well as the C−O(σ) and perhaps M−O(σ) ionizations on the low energy side of the region.

(20) Sanderson, R. T. *Simple Inorganic Substances;* Krieger: Malabar, FL, 1989.

Table 1. Relative Areas of the He I Spectra Regions (A, A*, B + C) of ^{t}BuOH and $(^t BuO)_3M{\equiv}N$ Relative to the Total Area (A + A* + B + C)

		$(RO)_3M{\equiv}N$		
	ROH	Cr	Mo	W
8.5−10.0 eV (A)	0.09	0.13	0.21	0.18
10.0−10.5 eV (A*)		0.065		
10.5−14.5 eV (B + C)	0.91	0.80	0.77	0.82

Not surprisingly, this region closely matches the corresponding region of ^{t}BuOH, with some broadening on the leading edge. Band B is fairly consistent as M is changed, once again implying dominant ligand character. However, subtle changes are apparent in the spectra that signal the presence of ionizations from orbitals containing some metal character. Not surprisingly, the leading bands (A + A*) of the spectra show the largest changes, implying that this region contains the ionizations from the orbitals that contain the most metal character.

It is useful to compare the relative areas of the ionization bands of the Cr, Mo, and W analogues, shown in Table 1. This is particularly helpful in showing that the ionization feature labeled A* in the $(^t BuO)_3Cr{\equiv}N$ spectrum shifts into band A in the spectra of the Mo and W compounds, because the relative area of combined A* + A agrees well with the relative areas of band A for $(^t BuO)_3M{\equiv}N$ (M = Mo or W). In terns of the molecular orbital model shown in Figure 3, band A contains the ionizations with antibonding character that form the first cluster of molecular orbitals ($2a_1$, 3e, a_2, and 2e), while band B contains the ionizations with bonding combinations of the M≡N σ and π with the ligand a_1 and e ($1a_1$ and 1e).

Focusing on the region containing the first cluster of ionizations, photoelectron spectra were re-collected in the 8.5−10.5 eV region, Figure 5, so that a more detailed analysis of the ionization features could be obtained. The ionization energies of the prominent features of the $(^t BuO)_3M{\equiv}N$ spectra are given in Table 2. The experimental trend for the onset of ionization[21] is W < Cr < Mo. For ionizations from similar orbitals containing metal character, the expected trend of ionization energy is W < Mo < Cr. Further evidence of this unexpected trend is obtained from the positions of the first band of each molecule, where the experimental trend in ionization energies follows as Cr < W < Mo. The observation that the Cr analogue does not fall in line with the Mo and W systems leads to the proposition that the first spectral feature of the Cr molecule is not due to ionization of an orbital containing Cr≡N σ and/or π character. From the molecular orbital considerations shown in Figure 3, the first ionization of $(^t BuO)_3Cr{\equiv}N$ more than likely corresponds to ionization of the a_2 ligand combination.

As mentioned before, this orbital is completely antibonding between the oxygen atoms, and shorter distances between the oxygen atoms will lead to a less stable orbital and lower ionization energy. On the other hand, since the first spectral features of the Mo and W analogues do follow the expected trend for metal-based ionizations, it is likely that the first ionization features of these molecules are due to ionization of orbitals containing some M≡N σ and/or π character, specifically the $2a_1$ and 3e orbitals in Figure 3. The ligand a_2 orbital, being completely nonbonding with respect to the metal, should be stabilized as one moves from Cr to Mo to W. Therefore, the ionization from the a_2 orbital more than likely occurs under feature b for the Mo analogue and under feature b or c for the W analogue. This then leaves band c to be tentatively assigned to the ionization of the other e combination, labeled 2e in Figure 3. The spectrum of the W complex gives evidence of spin−orbit splitting in this ionization as expected for this assignment.

(21) Onset of ionization (*) = ionization energy at which the amplitude is 10% of the maximum amplitude of the lowest energy Gaussian peaks used to fit each spectrum.

Table 2. Prominent Features in the He I Photoelectron Spectra and the Calculated Lowest Ionization Potentials (IPs) by ADF2007.01 [a]

$(RO)_3M{\equiv}N$		ionization energy (eV)				
M	R	ionization onset[30]	a	b	c	IP (calcd)
Cr	$(CH_3)_3C$	8.77	9.03	9.43/9.57	10.20	8.42
Mo	$(CH_3)_3C$	8.89	9.27	9.58	9.96	8.54
W	$(CH_3)_3C$	8.75	9.21	9.39/9.71	10.03/10.16	8.46
Mo	$(CH_3)_2HC$	9.10	9.48	9.85	10.26	8.76
Mo	$CF_3(CH_3)_2C$	9.73	10.36	10.36	10.91	9.45

[a] See Figure 4 for definitions of peaks.

He II Spectra. To provide additional evidence of the position of ionizations that contain M≡N σ and π character, the photoelectron spectra were re-collected using a He II photon source. Experimental cross-sections for ionizations from molecules roughly follow the trends predicted by the Gelius model, where molecular cross sections are treated as the sum of the atomic cross sections of the atoms that contribute to the

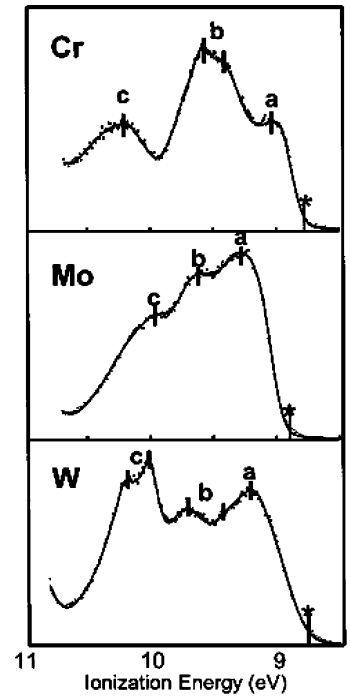

Figure 5. He I photoelectron spectra of $(^t BuO)_3M{\equiv}N$ (M = Cr, Mo, or W) in the 8−11 eV range. The major features in the spectra are labeled a, b, and c. The onset[30] of ionization is designated by an asterisk.

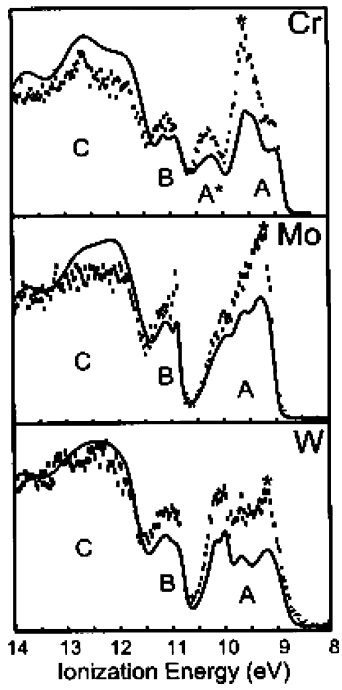

Figure 6. He II photoelectron spectra of (^{t}BuO)$_3$M≡N (M = Cr, Mo, or W). The data points are the He II spectra shown in comparison to the He I spectra (solid lines). The positions of the lowest energy ionizations with M≡N σ and π character are designated by an asterisk.

molecular orbital character.[22] Yeh and Landau have performed calculations to predict the cross-sectional behavior of the atomic elements.[22] The calculated valence atomic He II/He I ionization cross-section ratios for the atoms in these molecules are the following: H(0.153), C2p (0.306), N2p (0.4), O2p (0.639), F2p (0.905), Cr3d (0.925), Mo4d (0.323), and W5d (0.322). Although ionizations from Mo- and W-based orbitals are predicted to drop in intensity when He II is used as the photon source, experimentally they are known to gain in intensity under He II radiation.[23] The calculated cross-sections do not account for the Super-Koster Kronig transitions that occur for second and third row transition metals; these processes increase the intensity of ionizations from orbitals containing metal character.[23] Thus, in comparing He II spectra with He I spectra, ionizations with metal character are expected to grow with respect to those with oxygen and nitrogen character, which in turn are expected to grow with respect those with carbon and hydrogen character. The He II ionization intensities of the (RO)$_3$M≡N analogues in the 8−15 eV region are compared to the He I ionization intensities in Figure 6. The ionizations in the 8.5−11.5 eV region (bands A, A*, and B) grow in intensity relative to band C under He II radiation, consistent with substantial oxygen, metal, and nitrogen character in regions A and B and substantial C−C σ and C−H σ character in region C. Not surprisingly, the ionization between 8.0 and 10.5 eV (bands A and A*) shows the most growth in intensity when He II is used as the photon source, indicating the most metal character in the ionizations of this region.

Looking more closely at the (^{t}BuO)$_3$Cr≡N spectra, the most growth under He II radiation occurs around 9.5 eV (the high end of band A designated by an asterisk); therefore, the ionizations with Cr≡N σ and π character must occur in this region of the spectrum. This does not correspond to the first ionization feature of the Cr spectra. On the basis of this data, the first ionization does not correspond to ionization of a Cr-containing orbital, consistent with assignment of the first ionization of the Cr compound to the a_2 ligand combination. Looking at the 8.5−11.5 eV region of the Mo molecule, the most growth occurs in the beginning of band A under He II radiation. A similar conclusion is reached when looking at the spectra of the W molecule, although the intensity changes are not as pronounced. Spin−orbit coupling when orbitals are close in energy and contain W character will increase the mixing between orbitals and diminish the intensity effects. Nonetheless, the assignment of M≡N σ and π character to the first ionization feature of the Mo and W spectra is supported by the He II data analysis. Although the positions of the ionization containing the most metal character are identified in the He II spectral analysis, the overall growth in the region points toward extensive mixing between the M≡N orbitals and the alkoxide framework.

Ligand Substitution. Another useful technique for assigning ionizations in photoelectron spectroscopy is to study a series of molecules with varying ancillary ligands attached to the same transition metal center. In this particular instance, we have studied the (RO)$_3$Mo≡N molecules where R = C(CH$_3$)$_3$, CH(CH$_3$)$_3$, or CCF$_3$(CH$_3$)$_2$. This allows one to study the effects of alkoxide substitution on the electronic structure of the transition metal nitrides. The general layout of the spectra from 8.0 to 15.0 eV is unaffected by alkoxide substitution; the spectra still consist of three distinct regions: A, B, and C (see Figure 7). The spectral features all shift in accordance with the expected donor capacity of the alkoxide ligand: −OC(CH$_3$)$_3$ > −OCH(CH$_3$)$_2$> −OCCF$_3$(CH$_3$)$_2$. In general, the shifts correlate well with the shift of the lone pair ionizations of the free alcohols, where (CH$_3$)$_3$COH = 10.22 eV, (CH$_3$)$_2$HCOH = 10.36 eV, and (CH$_3$)$_2$(CF$_3$)COH = 11.11 eV. Although the overall layout of the spectra does not change as the alkoxide donor identity is changed, subtle changes are present in ionization band A, shown in Figure 8. The prominent ionization features in band A are labeled a, b, and c, and as seen in Table 2, these features shift in accordance with the overall donor ability of the alkoxide ligand. The cross-sectional changes seen in the (^{t}BuO)$_3$-Mo≡N He II spectrum are also seen in the He II spectra of the substituted alkoxide molecules (see Figure 9). The leading edge of band A grows substantially with respect to the rest of the spectrum for all of the substituted molybdenum nitrides. Hence, changing the alkoxide donor group serves only to shift the overall ionization energies in the spectra and the ionizations from the M≡N σ and π remaining the first ionizations of the molybdenum−nitride molecules.

Density Functional Studies. First, the gas phase geometries of the (^{t}BuO)$_3$M≡N molecules, where M = Cr, Mo, and W, were calculated by employing density functional

(22) Yeh, J. J.; Lindau, I. *At. Data Nucl. Data Tables* **1985**, *32*, 1.
(23) Green, J. C. *Acc. Chem. Res.* **1994**, *27*, 131.
(24) Chisholm, M. H.; Hoffman, D. M.; Huffman, J. C. *Inorg. Chem.* **1983**, *22*, 2903.

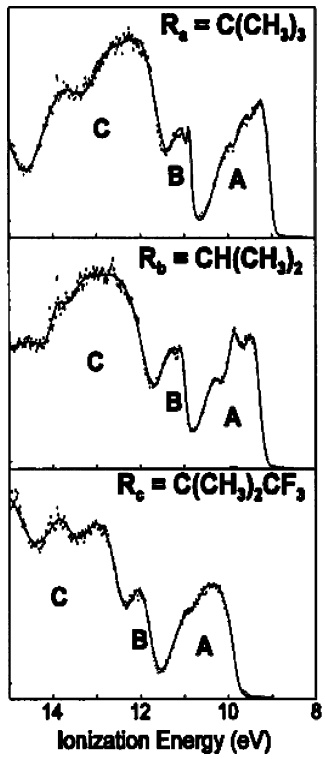

Figure 7. He I photoelectron spectra of $(RO)_3Mo{\equiv}N$ ($R_a = {}^tBu$, $R_b = {}^iPr$, $R_c = (CH_3)_2CF_3C$).

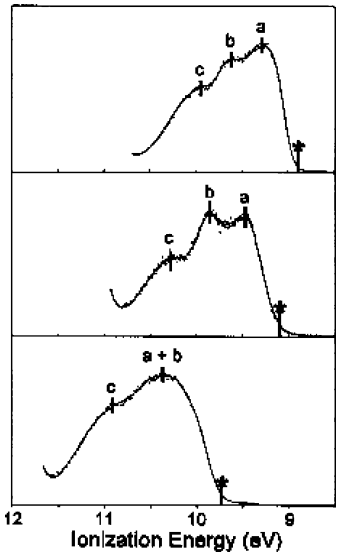

Figure 8. He I photoelectron spectra of $(RO)_3Mo{\equiv}N$, $R = {}^tBu$ (top), $R = {}^iPr$(middle), $R = CF_3(CH_3)_2C$ (bottom), from 8.5 to 12 eV. The major ionization features in the spectra are labeled a, b, and c. The onset of ionization is designated by an asterisk.

theory as implemented by ADF2007.01. Computational details are given in the Experimental and Computational Procedures section. The calculated bond distances and angles for the C_{3v} symmetric $(CO)_3M{\equiv}N$ cores are given in Table 3 where a comparison is made with their observed solid-state molecular structures.[16,17,24] Whereas the solid-state structure for M = Mo and W contains an infinite chain involving $(M{\equiv}N{\rightarrow}M{\equiv}N{\rightarrow})_\infty$ interactions with very long dative N→M bond distance >2.5 Å, the chromium containing molecule is discrete and thus might be expected to more closely represent the calculated gas phase structure. In

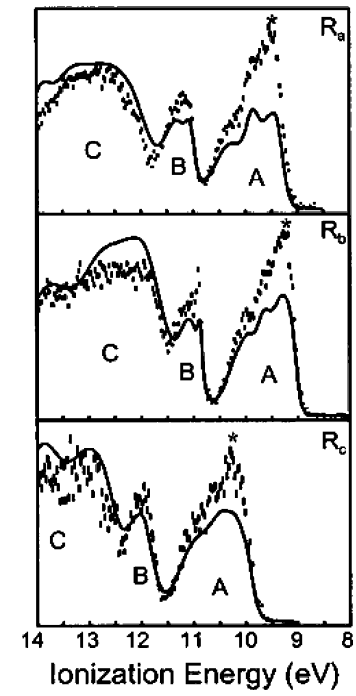

Figure 9. He II photoelectron spectra of $(RO)_3Mo{\equiv}N$ ($R_a = {}^tBu$, $R_b = {}^iPr$, $R_c = (CH_3)_2CF_3C$). The data points are the He II spectra shown in comparison to the He I spectra (solid lines). The positions of the lowest energy ionizations with M≡N σ and π character are designated by an asterisk.

Table 3. Comparison of the ADF2007.01 Optimized Geometrical Parameters with the Crystal Structure Parameters for $({}^tBuO)_3M{\equiv}N$

	Cr		Mo		W	
$({}^tBuO)_3M{\equiv}N$	expt	calcd	expt	calcd	expt	calcd
M−N (Å)	1.538	1.549	1.661	1.680	1.740	1.715
M−O (Å)	1.739	1.765	1.882	1.904	1.872	1.910
O−C (Å)	1.442	1.452	1.452	1.462	1.475	1.467
C−C (Å) (av)	1.499	1.530	1.522	1.529	1.526	1.528
N−M−O (deg)	108.2	109.1	103.3	107.4	101.6	107.3
M−O-C (°)	137.4	133.9	135.1	134.2	136.6	134.2
O−C−C (°) (avg.)	106.9	107.7	108.1	107.6	108.6	107.5
O O (Å)	2.86	2.890	3.17	3.146	3.18	3.159

Table 4. Calculated Orbital Energies (in eV) of the Highest Six Occupied Orbitals for $({}^tBuO)_3M{\equiv}N$

label	orbital makeup	Cr	Mo	W
a_2	OR (a_2)	−6.21	−6.44	−6.53
$2a_1$	M≡N σ − OR (a_1)	−6.59	−6.32	−6.27
3e	M≡N π and OR (e)	−6.54	−6.60	−6.40
2e	M≡N π and OR (e)	−7.07	−6.87	−6.83
1e	M≡N π and OR (e) and M (d_{xy}, $d_{x^2-y^2}$)	−7.80	−7.86	−7.82
$1a_1$	M≡N σ + OR (a_1)	−8.00	−7.95	−7.80

comparing the experimental and calculated structures, we note first the relative good agreement and then that the maximum deviations are seen for tungsten where the calculated W≡N distance is 1.715 Å and the observed is 1.740 Å. The observed lengthening of the W≡N bond in the solid-state structure may well rest with its strong dative bond.

The calculated orbital energies of the highest six occupied frontier orbitals for each of the metal containing nitrides are given in Table 4. The HOMOs, which are underlined in Table 4, follow the expected trend and indicate that, for M = Cr, the HOMO is indeed an alkoxide oxygen pπ combination of a_2 symmetry. We also note the calculations predict a

Table 5. Calculated Primary Orbital Characters for (^{t}BuO)$_3$M≡N

	Cr	Mo	W
a_2	76% O p	74% O p	73% O p
	17% C p	18% C p	19% C p
$2a_1$	3% N s	3% N s	6% N s
	37% N p	42% N p	53% N p
	4% Cr d_{z^2}	6% Mo d_{z^2}	10% W d_{z^2}
	34% O p	32% O p	18% O p
	15% C p	8% C p	4% C p
3e	7% N p	8% N p	43% N p
	7% Cr d_{xz}, d_{yz}	5% Mo d_{xz}, d_{yz}	19% W d_{xz}, d_{yz}
			2% W p
	56% O p	57% O p	20% O p
	17% C p	18% C p	6% C p
2e	32% N p	37% N p	9% N p
	11% Cr d_{xz}, d_{yz}	12% Mo d_{xz}, d_{yz}	2% W d_{xz}, d_{yz}
	3% Cr d_{xy} ,$d_{x^2-y^2}$	1% Mo d*xy*, $d_{x^2-y^2}$	
	5% Cr p	4% Mo p	2% W p
	25% O p	26% O p	56% O p
	12% C p	11% C p	15% C p
1e	12% N p	9% N p	5% N p
	12% Cr d_{xy}, $d_{x^2-y^2}$	10% Mo d_{xy},$d_{x^2-y^2}$	9% W d_{xy},$d_{x^2-y^2}$
	11% Cr d_{xz}, d_{yz}	9% Mo d_{xz},d_{yz}	6% W d_{xz}, d_{yz}
	10% O p	10% O p	15% O p
	36% C p	40% C p	44% C p
	12% H s	13% H s	14% H s
$1a_1$	3% N s	3% N s	2% N s
	23% N p	17% N p	10% N p
	26% Cr d_{z^2}	20% Mo d_{z^2}	15% W d_{z^2}
	2% Cr p	3% Mp p	2% W p
	6% O p	10% O p	19% O p
	26% C p	31% C p	34% C p
	8% H s	8% H s	12% H s

significant energy gap between the HOMO − 4 and HOMO − 5 orbitals of ∼1.0 eV. Thus, of the six occupied frontier orbitals, there is a set of four (a_2, $2a_1$, 3e, 2e) above two (1e, $1a_1$). The principal atomic orbital contribution of these frontier orbitals is given in Table 5.

In looking at the data shown in Table 5, one is struck by orbital mixing in what might formally constitute the metal−nitrogen triple bond as represented by the valence bond description M≡N. Only the a_2 orbital is in a sense easily described as a ligand based lone pair combination. The principal features of the M≡N σ component arise from $2a_1$ and $1a_1$ where it can be seen that for M = W $2a_1$ has a dominant contribution while for M = Cr it is the more stabilized $1a_1$ orbital. The M≡N π orbitals are seen to be extensively mixed with alkoxide ligand orbitals. The M≡N π bonding orbitals have e symmetry, and as can be seen from Table 5, the entries for chromium and molybdenum are similar and quite different from those for tungsten. For M = Cr and Mo, the metal d_{xz}, d_{yz} contribution is largely split between the 1e and 2e orbitals with the latter having the greater N 2p(π) character. For M = W, the 3e orbital carries the major contribution of metal d_{xz}, d_{yz} and N pπ orbitals. Despite the similarity in the frontier orbital atomic compositions for M = Cr and Mo, the relative energies of the orbitals are different. For M = Cr, the order is a_2 > 3e > $2a_1$; for M = Mo, $2a_1$ > a_2 > 3e; and for M = W, $2a_1$ > 3e > a_2. These are depicted in Figure 10. It is also particularly interesting to note the closeness in energy for (^{t}BuO)$_3$W≡N of the W≡N σ/lone pair with that of the W≡N π bonding MO.

A pictorial representation of the native of the key frontier orbitals is given in Figure 11. From these views, the $2a_1$ orbital for M = W is somewhat more extended toward the vacant site while the corresponding orbital for M = Cr is

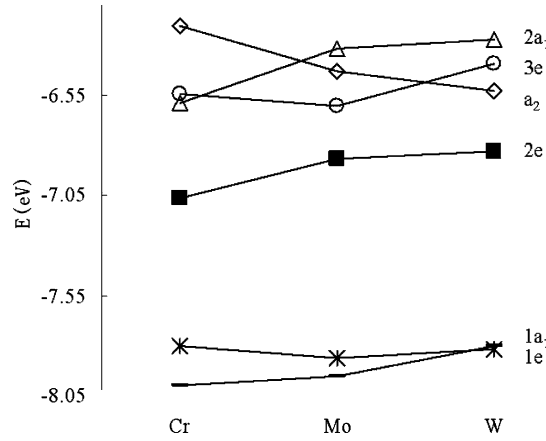

Figure 10. Correlation diagram of the Kohn−Sham orbital energies of (^{t}BuO)$_3$M≡N.

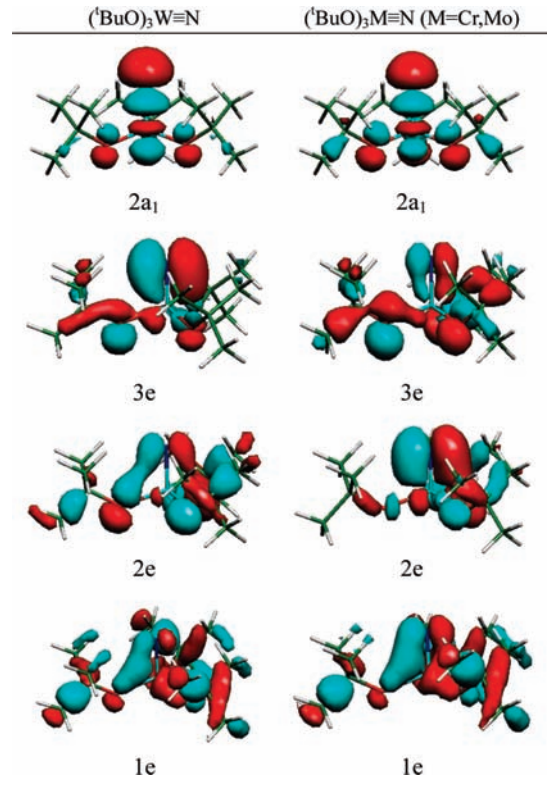

Figure 11. Molecular orbital plots of $2a_1$, 3e, 2e, and 1e valance orbitals (contour value = ±0.04) for (^{t}BuO)$_3$M≡N where M = Cr, Mo, and W. The orbital plots for molecules containing Cr and Mo are represented in the same set on the right because they look similar.

more delocalized. Although the change is subtle, it likely contributes to the observation that the (^{t}BuO)$_3$W≡N molecules are associated in the solid-state while the chromium analogue exists as a monomer. Also in Figure 11, the principal W≡N π bonding orbital is clearly seen to be the 3e orbital while for M = Cr, the π bonding is less obvious but is composed of parts of the 1e and 2e orbitals.

The calculated lowest ionization energies are given in Table 2 along with a comparison with the experimental values. In all cases the calculated ionization energies are smaller than the experimental values but differ by less than 1 eV. The calculated values correlated well with the experimental results with regard to the metal Cr < W < Mo and also the influence of the donating properties of the

Table 6. Mulliken Charge, Molecular Dipole Moment (μ), and M≡N Bond Dissociation Energy (BDE) Values Calculated by ADF2007.01 for $(RO)_3M{\equiv}N$

	$(^tBuO)_3M'N$			$(RO)_3Mo{\equiv}N$	
	Cr	Mo	W	$(CH_3)_2HC$	$CF_3(CH_3)_2C$
M	+1.51	+1.95	+2.00	+1.89	+1.97
N	−0.53	−0.63	−0.66	−0.60	−0.60
O	−0.67	−0.75	−0.77	−0.75	−0.75
μ (debye)	0.569	0.129	−0.417	−0.108	5.488
BDE (kcal/mol)	127.2	163.6	181.3	162.8	162.1

alkoxides $(CH_3)_3CO$ < $(CH_3)_2HCO$ < $(CF_3)(CH_3)_2CO$. The orbital origin of ionization is calculated to be for M = Cr, a_2; for M = Mo, $2a_1$; and for M = W, 3e. Thus, for tungsten we see an example of where Koopman's theorem breaks down as it does indeed for N_2. [However, strictly speaking, Koopman's theorem applies to Hartree−Fock orbital eigenvalues and not directly to Kohn−Sham orbital energies.] For $(^tBuO)_3W{\equiv}N$ we have the ground-state configuration $\cdots a_2^2(3e)^4(2a_1)^2$, and for $[(^tBuO)_3W{\equiv}N]^+$, $\cdots a_2^2(2a_1)^2(3e)^3$. For N_2 in its ground-state, the order is $\cdots(2\sigma_g)^2(1\pi)^4$, and for N_2^+, $\cdots(1\pi)^4(2\sigma_g)^1$. The calculated ionization energies for the W≡N $2a_1$ and 3e orbitals for M = W are 8.60 and 8.46 eV, respectively.

The calculations also produce a number of other interesting comparisons within this series. The results of Mulliken charges on the metal, nitrogen, and oxygen atoms are compared in Table 6 along with the molecules' dipole moments and M≡N bond dissociation energies. It is clearly seen that the effective positive charge on the metal and the negative charge on nitrogen increase down the series of the group 6 elements. This results in a change of sign of the dipole moment, but only for M = W is the sign negative because of the influence of the negative charges on the oxygen atoms. The reversed sign of the dipole moment for tungsten is the only example where the simple bond polarity of the metal−nitride bond, $M^{\delta+}-N^{\delta-}$, is seen to determine the overall direction of the dipole. In the case of $((CF_3)(CH_3)_2CO)_3Mo{\equiv}N$, the large positive dipole arises from the position of the three CF_3 groups in an anti configuration with respect to the W≡N bond.

The M≡N stretching frequencies were also calculated, and these followed the trend observed experimentally: Cr > Mo ∼ W, though the calculated and experimental values differed significantly. Experimental (calculated) frequencies in cm^{-1} follow: M = Cr, 1037 (1110); M = Mo, 1020 (1045); M = W, 1010 (1048). Rather interestingly, the experimental to calculated values of $\delta^{15}N$ (relative to $^{15}NH_3$) were in close agreement: M = Mo, 828 (822); M = W, 732 (735). The calculated value of $(^tBuO)_3Cr{\equiv}N$ was 935 ppm.

Conclusions

From the experimental and computational studies reported herein, the bonding in the molecules $(RO)_3M{\equiv}N$ can be understood in terms of extensions of the multiple bonding in N≡N and $CH_3C{\equiv}N$. However, unlike N_2 and CH_3CN, the present study indicates the importance of the alkoxide donors to the electronic structure. Because of extensive mixing with the oxygen orbitals, the $2a_1$ orbital of the tungsten and molybdenum analogues, which contains substantial $N(2p_z)$ character, contains little metal d_{z^2} character and is largely nonbonding. Therefore, this orbital is capable of donating electrons with little cost to the stability of the molecule. This explains the formation of the linear chains of the Mo and W molecules in the solid state with only small structural changes in the molecules. The HOMO of the chromium molecules is the highest-occupied alkoxide a_2 orbital because of the strong antibonding character between the oxygen atoms and the smaller metal atom that serves to provide short Cr−O and O−O distances. Therefore, the chromium molecule is easier to oxidize than would be anticipated in comparison to the molybdenum and tungsten molecules.

Both the charge distribution of the molecules and the N atom basicity are directly dependent on the identity of M. The polarization of the M≡N bond increases as M = Cr < Mo < W. Hence, the basicity of the N-atom also increases in the same order. Because the $2a_1$ orbital of the Cr molecules is not the HOMO and the N atom is less basic in the Cr molecule than in the Mo and W molecules, the Cr molecule has less tendency to form linear chains in the solid state.

The substitutions on the alkoxide donor ligands studied here have little effect on the electronic structure of the $(RO)_3Mo{\equiv}N$ molecules other than shifting all of the ionization energies together, again pointing to the extensive delocalization of the molecular orbitals. The orbital compositions and relative orbital positions are not substantially changed because all of the orbitals are shifted similarly in accordance with the overall donor ability of the alkoxide ligand.

The reactivity of the transition metal nitrides, analogous to that of the organic nitriles, is not particularly surprising in light of this understanding of the electronic structure and bonding. The W≡N molecule not only has the greatest charge dipole ($M^{\delta+}-N^{\delta-}$) but also the greatest N-atom basicity. The M≡N bond strength increases as M = Cr < Mo < W. However, as recent work has shown the lability of the M≡N bond to enter into nitrogen atom metathesis with organic nitriles follows the inverse order W > Mo ≫ Cr. This underscores the importance of not relating thermodynamics of bonds to their kinetic lability.

Experimental and Computational Procedures

General Methods. All manipulations were carried out using an argon (Ar) or dinitrogen (N_2) atmosphere and standard air and moisture sensitive techniques in a Vacuum Atmospheres glovebox or Schlenk line. Solvents were distilled from CaH_2 or Na/Benzophenone ketyl, purged of oxygen with either Ar or N_2, and stored over 4 Å sieves. All reagents were purchased from Aldrich unless otherwise stated and were used without further purification. *tert*-Butanol was vacuum distilled from $CaSO_4$.

Fluoroalcohols (Lancaster Synthesis) were distilled under Ar and stored over 4 Å sieves. Molybdenum pentachloride (Strem Chemicals) was used as purchased. Lithium, sodium, or potassium alkoxide and fluoroalkoxide salts were prepared using a reported method.[25] Molybdenum tetrachloride bisacetonitrile ($MoCl_4$-

(25) Samuels, J. A.; Lobkovsky, E. B.; Folting, K.; Huffman, J. C.; Zwanziger, J. W.; Caulton, K. G. *J. Am. Chem. Soc.* **1993**, *115*, 5093.

($CH_3CN)_2$) was prepared via a reported method.[26,27] The compounds (^{t}BuO)$_3$MN, where M = Cr, Mo, W, and M$_2$(O^tBu)$_6$, where M = Mo and W, were prepared via reported syntheses.[16,18,28,29] The molybdenum nitrido alkoxides and fluoroalkoxides were prepared via modification of a reported synthesis.[17]

Spectroscopic Methods. Proton (^{1}H) and fluorine (^{19}F) NMR data were obtained with a Varian Gemini 2000 spectrometer operating at a 300 MHz proton and 282 MHz fluorine NMR Larmor frequencies. Infrared (IR) spectra were taken as KBr pellets on a Nicolet 510P FT-IR spectrophotometer using OMNI E.S.P. software. Mass spectra were taken on a Kratos MS 80 high resolution mass spectrometer using negative ion CI with methane (CH_4) as reagent gas. A Kratos MS 25 RFA double focusing magnetic sector mass spectrometer was also used to record the missed metal spectrum. A positive ion EI source with a trap current of 100 μA was used at a temperature of 225 °C at 52 eV. A 3 kV analyzer was used with a resolution of 2000 using the 5% peak height definition. The scanning rate was 5 s/decade with a mass range 1100−275. A third party (MSS) data system was used.

Photoelectron Spectra. The photoelectron spectra were recorded using an instrument that features a 36 cm radius, 8 cm gap McPherson hemispherical analyzer with custom-designed sample cells, detection system, and control electonics.[30] The excitation source was a quartz lamp with the ability, depending on operating conditions, to produce He Iα (21.218 eV) or He IIα (40.814 eV) photons. The ionization energy scale was calibrated by using the $^2E_{1/2}$ ionization of methyl iodide (9.538 eV). The argon $^2P_{3/2}$ ionization was also used as an internal calibration lock for the energy scale during He I and He II data collection runs. Resolution (measured as full-width-at-half-maximum of the argon $^2P_{3/2}$ ionization) was 0.016−0.024 eV during He I data collection. Assuming a linear dependence of analyzer intensity on the kinetic energy of the electrons within the energy range of these experiments, all data were intensity corrected with the experimentally determined analyzer sensitivity function.

Because discharge sources are not monochromatic,[31] each spectrum was corrected for the presence of ionizations from other source lines. The He I spectra were corrected for ionizations from the He Iβ line (1.957 eV) higher in energy with 3% of the intensity of ionizations from the He Iα line. He II spectra were similarly corrected for ionizations from the He IIβ line (7.568 eV higher in energy and 12% of the intensity of the He IIα line.)

The samples sublimed cleanly with no detectable evidence of decomposition products in the gas phase or as solid residue. The sublimation ranges (°C at ∼10^{-4} Torr) for each molecule were (^{t}BuO)$_3$Cr≡N, −4 to 20; (^{t}BuO)$_3$Mo≡N, 38 to 57; (^{t}BuO)$_3$W≡N, 58 to 78; (^{i}PrO)$_3$Mo≡N, 42 to 75; (Me$_2$CF$_3$CO)$_3$Mo≡N, 28 to 61. The temperatures were measured using a "K" type thermocouple attached directly to the ionization cell through a vacuum feedthrough.

Data Analysis. In the figures of the photoelectron spectra, the vertical length of each data mark represents the experimental variance of that point.[32] The ionization bands are represented analytically with the best fit of asymmetric Gaussian peaks. Due to the extensive overlap of many ionization features, the individual peaks used to obtain an analytical representation of a band do not necessarily represent separate ion states. The number of peaks used was the minimum necessary to get an analytical representation of the He I spectrum. For fitting the He II spectra, the peak positions and half-widths were fixed to those of the He I fit, and only the relative intensities were allowed to vary.

The confidence limits for the relative integrated peak areas are ±5%. The primary source of uncertainty is the determination of the baseline. The baseline is caused by electron scattering and is taken to be linear over the small energy range of these spectra. The fitting procedures used to fit the spectra have been described in more detail elsewhere.[32]

Computational Details. All DFT calculations were performed using the Amsterdam Density Functional (ADF) software package, version 2007.01,[33] developed by Baerends and co-workers.[34] The numerical integration scheme used was developed by te Velde et al.,[35] and the geometry optimization procedure was based on the method of Versluis and Ziegler.[36] All geometry optimizations were carried out under C_{3v} symmetry by using the local exchange-correlation potential of Vosko et al.[37] and the nonlocal exchange and correlation corrections of Perdew and Wang (PW91).[38] All atoms were described using a triple-ζ Slater type orbital (STO) basis set with one polarization function (TZP); the core was frozen at the 2p, 3d, and 4f level for chromium, molybdenum, and tungsten, and 1s for the second row atoms. All atoms were corrected for scalar relativistic effects by using the zeroth order regular approximation (ZORA) method.[39] All calculations utilized an INTEGRATION value of 6; geometries were converged to a gradient of 10^{-3} au/Å. The self-consistent field energy was converged to a value of 10^{-6}. Frequencies were calculated by numerical differentiation of energy gradients in slightly displaced geometries using double-sided displacements.[40] Molecular orbitals were visualized with the molecular graphics package MOLEKEL, a free utility from the Swiss Center for Scientific Computing.[41] The plots were created with an isosurface value of ±0.04.

IC801786U

(26) Dilworth, J. R.; Richards, R. L. *Inorg. Synth.* **1980**, *20*, 119.
(27) Allen, E. A.; Brisdon, B. J.; Fowles, G. W. A. *J. Chem. Soc.* **1964**, 4531.
(28) Chisholm, M. H.; Cotton, F. A.; Murillo, C. A.; Reichert, W. W. *Inorg. Chem.* **1977**, *16*, 1801.
(29) Akiyama, M.; Chisholm, M. H.; Cotton, F. A.; Extine, M. W.; Haitko, D. A.; Little, D.; Fanwick, P. E. *Inorg. Chem.* **1979**, *18*, 2266.
(30) Lichtenberger, D. L.; Kellogg, G. E.; Kristofzski, J. G.; Page, D.; Turner, S.; Klinger, G.; Lorenzen, J. *Rev. Sci. Instrum.* **1986**, *57*, 2366.
(31) Turner, D. W.; Baker, C.; Baker, A. D.; Brundle, C. R. *Molecular Photoelectron Spectroscopy*; Wiley-Interscience: New York, 1970.
(32) Lichtenberger, D. L.; Copenhaver, A. S. *J. Electron. Spectrosc. Relat. Phenom.* **1990**, *50*, 335.
(33) *ADF 2007.01;* SCM, Theoretical Chemistry, Vrije Universiteit: Amsterdam, The Netherlands; http://www.scm.com.
(34) (a) Baerends, E. J.; Ellis, D. E.; Ros, P. *Chem. Phys.* **1973**, *2*, 41. (b) te Velde, G.; Baerends, E. J. *J. Comput. Phys.* **1992**, *99*, 84. (c) Fonseca Guerra, C.; Snijders, J. G.; te Velde, G.; Baerends, E. J. *Theor. Chim. Acc.* **1998**, *99*, 391. (d) Bickelhaupt, F. M.; Baerends, E. J. *Rev. Comput. Chem.* **2000**, *15*, 1. (e) te Velde, G.; Bickelhaupt, F. M.; Fonseca Guerra, C.; van Gisbergen, S. J. A.; Baerends, E. J.; Snijders, J. G.; Ziegler, T. *J. Comput. Chem.* **2001**, *22*, 931.
(35) Boerrigter, P. M.; teVelde, G.; Baerends, E. J. *Int. J. Quantum Chem.* **1998**, 87.
(36) Verslius, L.; Ziegler, T. *J. Chem. Phys.* **1998**, *88*, 322.
(37) Vosko, H.; Wilk, L.; Nusair, M. *Can. J. Phys.* **1980**, *58*, 1200.
(38) Perdew, P. *Phys. Rev. B.* **1992**, *46*, 6671.
(39) VanLenthe, E.; Ehlers, A. E.; Baerends, E. J. *J. Chem. Phys.* **1999**, *110*, 8943.
(40) (a) Fan, L.; Ziegler, T. *J. Chem. Phys.* **1992**, *96*, 9005. (b) Fan, L.; Ziegler, T. *J. Am. Chem. Soc.* **1992**, *114*, 10890.
(41) (a) Flükiger, P. Lüthi, H. P.; Portmann, S. ; Weber; J. *MOLEKEL4.3*; Swiss Center for Scientific Computing: Manno, Switzerland, 2000−2002. (b) Portmann, S.; Lüthi, H. P. *Chimia* **2000**, *54*, 766.